CHEMISTRY OF MATERIALS
Article
Cite This: Chem. Mater. 2018, 30, 1417−1426
pubs.acs.org/cm

Mixed Conductive Soft Solids by Electrostatically Driven Network Formation of a Conjugated Polyelectrolyte

Scott P. O. Danielsen,[†,‡] Gabriel E. Sanoja,[†,‡,§,¶] Samantha R. McCuskey,[†,‡] Boualem Hammouda,[∥] Guillermo C. Bazan,[‡,⊥,#] Glenn H. Fredrickson,*[,†,‡,⊥] and Rachel A. Segalman*[,†,‡,⊥]

[†]Department of Chemical Engineering, [‡]Materials Research Laboratory, [⊥]Materials Department, and [#]Department of Chemistry and Biochemistry, University of California, Santa Barbara, California 93106, United States

[§]Department of Chemical and Biomolecular Engineering, University of California, Berkeley, California 94720, United States

[∥]Center for Neutron Research, National Institute of Standards and Technology, 100 Bureau Drive, Gaithersburg, Maryland 20899, United States

Supporting Information

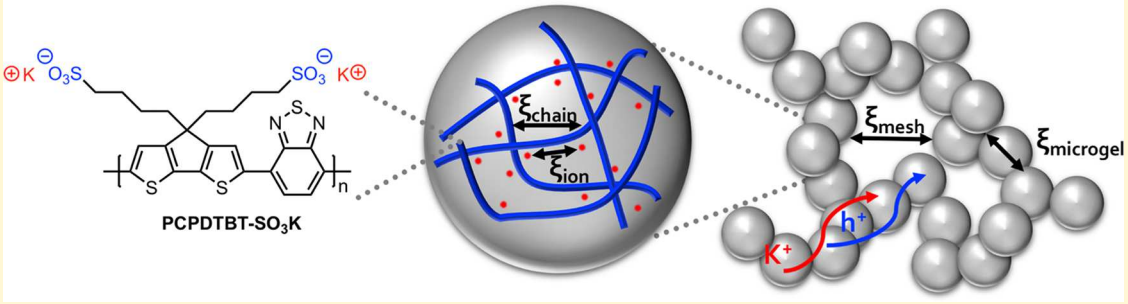

ABSTRACT: A conjugated polyelectrolyte (poly[2,6-(4,4-bis-potassium butanylsulfonate-4*H*-cyclopenta-[2,1-b;3,4-b']-dithiophene)-*alt*-4,7-(2,1,3-benzothiadiazole)], PCPDTBT-SO_3K) assembles into a novel, hierarchical hydrogel structure with all structural evidence indicating dominant electrostatic rather than aromatic or mesogen interactions. PCPDTBT-SO_3K forms an entangled polymer mesh, where polymer chains are tied together by ionic cross-links, comprising microgel clusters that percolate to form a macroscopic three-dimensional network. With increasing temperature, ions gain mobility to move toward the exterior of the microgel clusters, dissolving the ionic cross-links and inhibiting network percolation through electrostatic repulsion. While $\pi-\pi$ stacking interactions may be present in a disorganized fashion, no long-range $\pi-\pi$ stacking is evident in X-ray scattering. Soft materials based on PCPDTBT-SO_3K remain semiconducting and exhibit elevated ionic conductivity at the structural reorganization temperature.

INTRODUCTION

Conjugated polyelectrolytes (CPEs) combine a π-conjugated polymer backbone with pendant ionic groups to create water-soluble semiconductors.[1] The aqueous solubility provides an opportunity to form functional hydrogel structures for interfacing with biology.[2−4] Modulation of the chemistry of the polymer backbone enables tunability of charge transport, ionization potential, and optical properties. Ionic groups and charge compensating counterions allow control over solubility, charge transport, molecular packing, and solution aggregation.[5] Studies to understand the structure−property relationships of CPEs have led to increased chemical diversity and a variety of new synthetic protocols for controlled materials chemistry.[6,7] The breadth of developed CPEs has inspired work into their application in biological and chemical sensors[8−12] and organic optoelectronic devices, including light-emitting diodes (LEDs),[13,14] light-emitting electrochemical cells (LEECs),[15] photovoltaic devices,[16] and light-emitting transistors (LETs).[17] Despite the key role CPEs could play in energy conversion and storage, their solution and hydrogel structures and resulting physiochemical material properties remain largely unknown.

Poly[2,6-(4,4-bis-potassium butanylsulfonate-4*H*-cyclopenta-[2,1-b;3,4-b']-dithiophene)-*alt*-4,7-(2,1,3-benzothiadiazole)], PCPDTBT-SO_3K (Figure 1) is an attractive model system for elucidating the structure−property relationships of CPEs. Side-

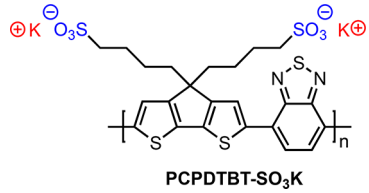

Figure 1. Chemical structure of PCPDTBT-SO_3K.

Received: December 21, 2017
Revised: February 3, 2018
Published: February 15, 2018

DOI: 10.1021/acs.chemmater.7b05303
Chem. Mater. 2018, 30, 1417−1426

chain and counterion modifications have allowed these CPEs to be instructive model systems for understanding the factors contributing to thermoelectric performance and electronic conductivity.[18,19] In particular because the anionic, narrow-band gap conjugated polyelectrolyte self-dopes in aqueous solution to form a water-soluble, stable, conductive polymer,[20] PCPDTBT-SO_3K has increased performance in a variety of optoelectronic applications, attributed to increases in interfacial contact and surface coverage between device layers.[21−24]

CPE hydrogels and solution structures pose an opportunity for improved interfacial contact in bioelectrochemical cells[2] and bioelectronics, particularly in neural interfaces.[3] Utilizing the advantageous interfacial modifying properties of CPEs as soft, conductive matrices at the abiotic−biotic interface[4] has increased conversion efficiencies in bioelectrochemical cells through improved contact between the microorganisms and the electrodes.[2] However, little is known about the structure of soft conductive CPE matrices.

The interconnection between structure and macroscopic photophysical properties has been explored in neutral conjugated polymers, yet as opposed to CPEs, these are absent of appreciable electrostatic interactions. The hierarchical assembly (i.e., network formation) of these materials in poor and concentrated solutions is driven by aromatic interactions yielding $\pi-\pi$ stacked, crystalline sheet-like aggregates embedded in an entangled polymer mesh.[25−27] Because CPEs incorporate more complex and interchain interactions, their microstructure should be driven not only by a combination of chain rigidity and aromatic interactions but also by electrostatic and hydrophobic effects in an aqueous solvent. Recent studies have suggested that semidilute solutions[28,29] and soft solids[30] of CPEs might form polyelectrolyte micelles that percolate to yield aggregates at long length scales. The micellar conformation has been suggested to result from the amphiphilic nature of CPEs and presumed backbone $\pi-\pi$ stacking interactions. However, the delicate balance of the competitive interactions that result in structure formation remain poorly understood. The electrostatic interactions between charged polymer segments are repulsive, although partially screened by the environment, while $\pi-\pi$ and other hydrophobic interactions are net attractive. Ionic cross-linking is also possible, engaging counterions as intermediaries between charged backbone units and representing a net attraction among chain segments. The balance of attractive and repulsive interactions allows for finite sized aggregates that under some conditions can percolate into extended networks.

Herein, we seek a more comprehensive understanding of the interplay between the different molecular interactions on the structure and critical transitions of a CPE hydrogel across a temperature range relevant for use as a processable, conductive, soft matrix. PCPDTBT-SO_3K is used to explore the interactions that lead to assembly and network formation of conjugated polyelectrolytes in aqueous solution at moderate concentrations. In particular, by investigating the structure of a PCPDTBT-SO_3K hydrogel across a range of temperatures, the electrostatic interactions are found to dominate the structural ordering. Finally, because the percolated microgel pathway within these systems is demonstrated to provide a scaffold for both ionic and electrical conductivity, such conjugated polyelectrolyte hydrogels are well-suited for applications in bioelectronics.

RESULTS AND DISCUSSION

This work illustrates the relative dominance of electrostatic interactions in determining the microstructure of soft materials formed by PCPDTBT-SO_3K in the semidilute concentration regime. A novel, multilength scale structure of PCPDTBT-SO_3K hydrogels is proposed, and a mechanism for structural transitions is presented. PCPDTBT-SO_3K, a semiflexible polymer, is observed in aqueous solution to form clusters of entangled polyelectrolyte mesh held together by ionic physical cross-links. The PCPDTBT-SO_3K hydrogel disorders upon heating due to the dissolution of ionic aggregates and the resulting electrostatic dispersion of clusters from forming a percolated polymer network. Finally, PCPDTBT-SO_3K hydrogels are mixed conductors capable of long-range, bulk electron and ion transport required for inclusion in energy conversion devices.

Solidification and Morphology. Increasing the concentration of PCPDTBT-SO_3K in aqueous solution past a critical threshold results in a well-formed hierarchical microstructure at low polymer fractions. We restrict our study to PCPDTBT-SO_3K (M_w= 11 000 g mol^{-1}, absolute weight-average molecular weight from small-angle neutron scattering (SANS) zero-angle scattering, Figure 3 and Table S2; Đ = 1.1 by SEC according to PS standards) hydrogels formed from semidilute solution at a concentration of 4.0% w/v in H_2O. The microstructure of the material, as illustrated by freeze−fracture scanning electron microscopy (FF-SEM) images in Figures 2a and b, is based on microgel units, where the polymer is assembled into spherical domains of 3−5 μm, which then interconnect to form a bulk three-dimensional network with mesh sizes of 10−20 μm. Noteworthy, the void size is ideal for the diffusion of nutrients and movement of bacteria: a requirement for the development of CPEs as interfacial modifying agents in bioelectrochemical cells.

The spanning of microgel aggregates appears to be a jamming of the particles, giving rise to the macroscopic mechanical properties characteristic of soft materials (e.g., hydrogels). The PCPDTBT-SO_3K remains a gel-like elastic solid at 25 °C (i.e., $G' > G''$ over the accessible frequency range), in the sense that it can sustain static loads and store elastic energy over long times. It exhibits an elastic modulus of order 10^3 to 10^4 Pa and a terminal relaxation time of 100s of seconds which, within the experimentally accessible times, are remarkably similar to traditional cross-linked polymer gels albeit with differences in microstructure. Although physically cross-linked polymer gels and the hydrogel soft material presented here are three-dimensional networks, the former is comprised of polymer chains joined together at a number of covalent connection sites, whereas the latter results from microgel clusters that percolate to form a macroscopic network. Noteworthy, the dynamical frequency sweeps, Figure 2c, are qualitatively consistent with the jamming of microgels, as indicated in the microscopy images and recent work on the jamming transitions of soft polyelectrolyte microgel suspensions.[31]

The existence of spherical microgels jamming to form a three-dimensional network is incompatible with the solution assembly of conjugated polymer and polyelectrolyte gels highlighted earlier.[30] As demonstrated with a combination of electron microscopy and rheology (Figure 2), the polymers are not associating into large crystalline aggregates or wormlike micelles. Thus, it is necessary to further interrogate the role of

DOI: 10.1021/acs.chemmater.7b05303
Chem. Mater. 2018, 30, 1417−1426

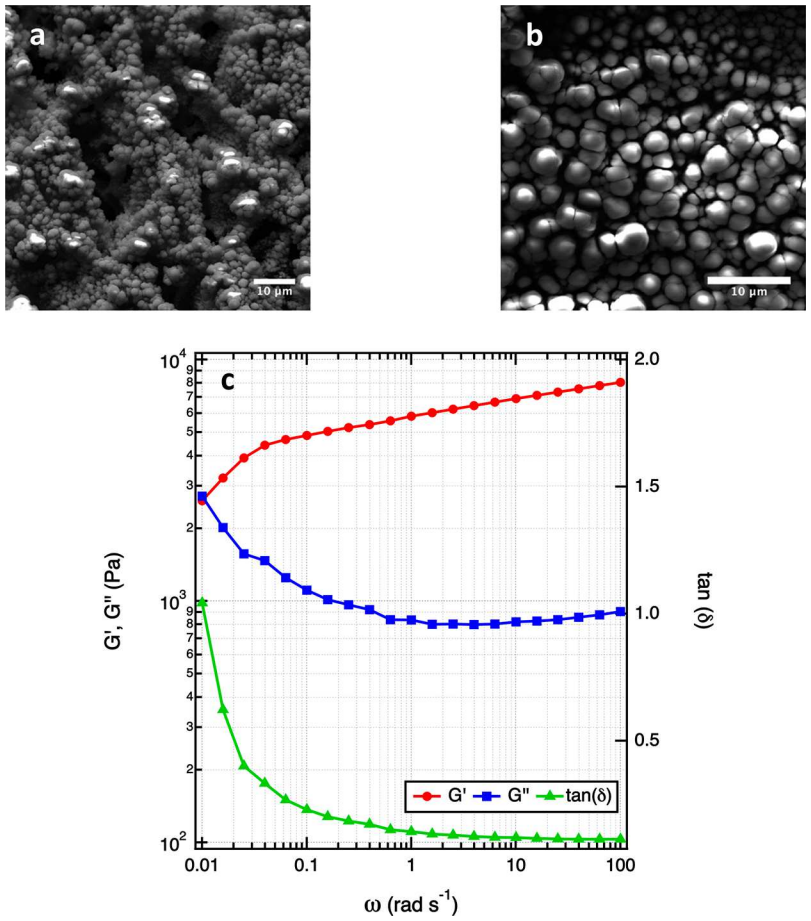

Figure 2. (a and b) FF−SEM images of PCPDTBT-SO_3K hydrogels (4.0% w/v, H_2O) and (c) dynamical frequency sweep of a PCPDTBT-SO_3K hydrogel (4.0% w/v, H_2O) at 25 °C.

aromatic and mesogen driven interactions in the microstructure of CPE semidilute solutions and hydrogels.

Chain Rigidity Effects. To elucidate chain rigidity effects on the structure of semidilute solutions of CPEs, it was crucial to understand the chain conformation of PCPDTBT-SO_3K. By operating in the dilute limit where polymer chains can be considered noninteracting, SANS can be used to extract information regarding correlations along a single polymer chain (i.e., form factor).

Conjugated polymers typically adopt configurational states that more closely resemble rigid rods than Gaussian coils. The Wormlike Chain model (WLC), or Kratky−Porod model, provides a useful form factor in describing these semiflexible systems.[32,33] The WLC model details a chain of contour length, L_c, as a sequence of locally stiff segments of persistence length, l_p. Persistence length is the length over which the chain maintains correlation to itself or, restated, the length over which the flexible cylinder can be considered a rigid rod. A WLC description models backbone stiffness in terms of the Kuhn length, $b = 2l_p$, as each Kuhn segment can be simulated as freely jointed with each other.

It is useful to compare the expected semiflexible behavior against both rigid rod and Gaussian coil descriptions as a confirmation of the chain behavior and characteristic lengths, highlighting good agreement of the SANS scattering data (Figure 3) with the WLC model across a wide q-range. PCPDTBT-SO_3K is a semiflexible polymer having a Kuhn length of (13.4 ± 0.9) nm and a cylinder radius of (1.4 ± 0.1) nm, as determined from a WLC fit[34,35] to the SANS scattering profile for PCPDTBT-SO_3K (dilute solution, 0.3% w/v, D_2O) presented in Figure 3.

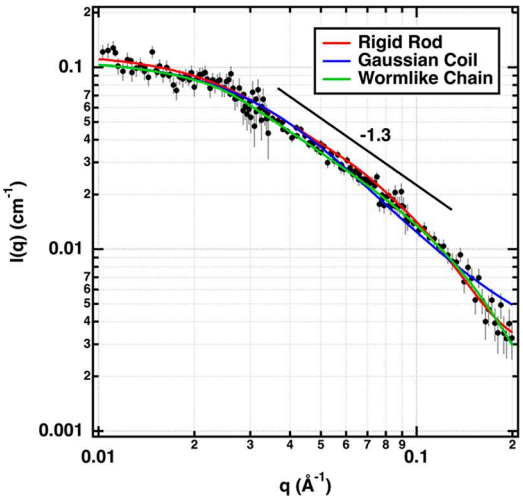

Figure 3. SANS data (●) with Rigid Rod (red −), Gaussian coil (blue −), and WLC model fit (green −) for PCPDTBT-SO_3K in dilute solution (0.3% w/v, D_2O).

PCPDTBT-SO_3K is thus significantly more rod-like than classical polymers.[36] It is also several times stiffer than poly(3-alkylthiophenes), P3ATs, due to the absence of syn−anti isomerism between thiophene units.[37] Although chain stiffness

DOI: 10.1021/acs.chemmater.7b05303
Chem. Mater. 2018, 30, 1417−1426

has historically been associated with the fused aromatic ring structure of the backbone and the electrostatics of the pendant ionic groups, PCPDTBT-SO_3K has a persistence length similar to neutral conjugated polymers such as poly(2-methoxy-5-(2′-ethylhexyloxy)-*p*-phenylenevinylene), MEH-PPV,[38,39] and polyfluorene, PF,[40] even with the high density of charges along the polymer.[41] Thus, electrostatic repulsions appear unimportant in dictating the stiffness of a chain as long as the backbone is conjugated. These comparisons allow coarse-graining of PCPDTBT-SO_3K as a semiflexible polymer, likely due to the finite backbone torsion and nonzero bond angles between donor (cyclopentadithiophene, CPDT) and acceptor (benzothiadiazole, BT) monomer units.

The semiflexible conformation, rather than rigid rod, is suggestive of the unimportance of chain rigidity effects compared to electrostatics in determining the structure and length scales of interactions of the soft solid (4.0% w/v). This is further illustrated by calculating critical concentrations in the Gaussian coil and rigid rod limits, in the absence of additional interactions.[42,43] In the Gaussian coil limit, the size of the polymer is well-described using the radius of gyration, R_g, with an overlap concentration,

$$c^*_{coil} \sim \frac{M/N_A}{\frac{4}{3}\pi R_g^3} \approx 4.3\%\ \text{w/v} \quad (1)$$

where M is the absolute weight-average molecular weight of the polymer determined from the zero-angle scattering of the SANS data, N_A is Avogadro's number, and the radius of gyration used was determined by the SANS fit to the Debye model (Figure 3 and Table S1).

Conversely, in the rigid rod limit, the overlap concentration depends on the volume accessible to a rotating cylinder,[42,43]

$$c^*_{rod} \sim \frac{M/N_A}{L_c^3} \approx 2.6\%\ \text{w/v} \quad (2)$$

where cylinder length L_c was determined by the SANS fit to the rigid rod model (Figure 3, Table S3). In this rigid rod limit, it is also useful to calculate the critical concentration for the isotropic to nematic transition,[42,43]

$$c^{**}_{iso\rightarrow nematic} \sim \frac{M/N_A}{dL_c^2} \approx 8.1\%\ \text{w/v} \quad (3)$$

where d is the diameter of the rod determined from the SANS fit to the rigid rod model (Table S3). Considering the chain length and stiffness for the PCPDTBT-SO_3K chains studied yield remarkably similar overlap concentrations in both the Gaussian and rigid rod limits and, comparable to the polymer concentration investigated, the chain interactions of a solution of PCPDTBT-SO_3K (4.0% w/v, H_2O) are anticipated to be characteristic of the semidilute regime. However, the hydrogels are sufficiently below the predicted isotropic to nematic transition, and thus presumably the mesogen interactions are of little structural or thermodynamic consequence.

Aromatic Interactions. Upon examining the local interactions of the PCPDTBT-SO_3K chains in their hydrogel environment via wide-angle X-ray scattering (WAXS), we observe the striking lack of diffraction peaks or $\pi-\pi$ stacking (Figure 4). Any local interchain contacts, including π-orbital overlap, must be weak or relatively disordered. Further, the absence of $\pi-\pi$ stacking or regularly ordered, close packed interchain correlations suggest the CPEs are not behaving

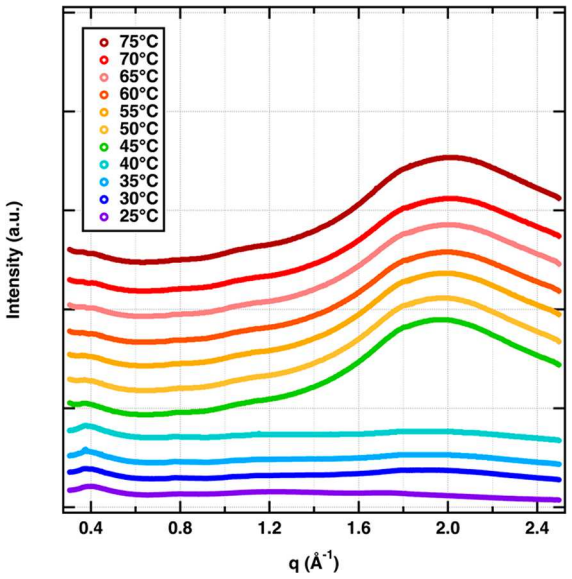

Figure 4. WAXS data for PCPDTBT-SO_3K hydrogels (4.0% w/v, H_2O) from 25−75 °C. Error bars are smaller than markers. The curves are arbitrarily shifted for clarity.

according to the proposed micellar model as amphiphilic polymers that associate hydrophobic conjugated backbones to arrange hydrophilic ionic side-chains out toward the bulk solvent.[30] The free energy penalty associated with the loss of entropy from water ordering in the solvation shell around the polymer (i.e., hydrophobic effect) appears less than the electrostatic energy penalty that would be required to associate the ionic groups so closely together in an ordered micellar arrangement. However, while not the dominant driving force for network formation, unstructured aromatic interactions likely contribute to the overall structure and conductivity pathways.

Electrostatic Interactions. Instead of $\pi-\pi$ stacking and chain stiffness effects dominating the structural ordering, electrostatics appear to be the primary driving force for solution assembly and solidification. The local correlations evident upon heating PCPDTBT-SO_3K hydrogels (4.0% w/v, H_2O) (Figure 4) are associated with electrostatic assembly, particularly given the relatively broad peaks that are classically a signature of ionic interactions. The broad peak centered at q = 2.0 Å^{-1} is associated with an approximately 3 Å solvation layer of the polymer chains. The narrower peak at q = 0.4 Å^{-1} corresponds to the presence of approximately 1.6 nm ionic clusters. Polarizability contrast between the conjugated polymer backbone, pendant ionic charges, counterions, and bulk aqueous solvent result in a nonuniform dielectric contrast, causing the ions to aggregate in semidilute solution. The aggregation of multiple ions serves to physically cross-link the chains together in entangled polyelectrolyte mesh clusters. With increasing temperature, the ionic aggregates dissociate, effectively un-cross-linking the polymer chains and disordering the microstructure. This greater solubilization of polymer chains causes a concomitant rise in intensity of a broad amorphous solvation peak. The dissociation of ionic cross-links and increase in polymer solvation occur over a narrow temperature range, 40 to 45 °C, agreeing well with additional scattering and conductivity measurements (Figures 7 and 8).

These local interactions complement the interpretation of larger length scale correlations. Figure 5 presents SANS profiles for 4.0% w/v PCPDTBT-SO_3K in D_2O at two temperatures, 25

DOI: 10.1021/acs.chemmater.7b05303
Chem. Mater. 2018, 30, 1417−1426

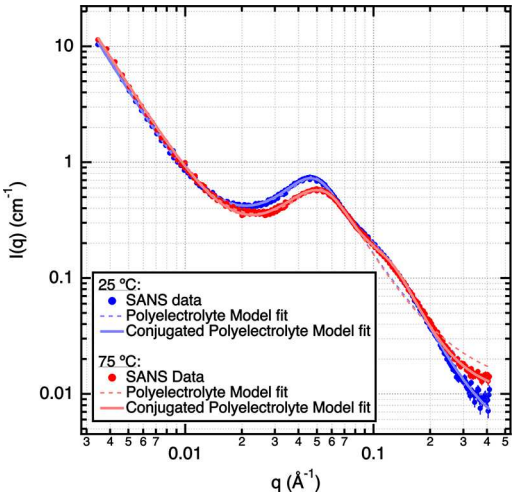

Figure 5. SANS data (●), fits to our conjugated polyelectrolyte model (−), and fits to the polyelectrolyte model (--) for PCPDTBT-SO_3K hydrogels (4.0% w/v, D_2O) at 25 °C (blue ●, −, --) and 75 °C (red ●, −, --). Outside of high-q data points, error bars are smaller than markers.

and 75 °C, where elastic and viscous behavior are observed, respectively. To extract correlation lengths and other relevant structural parameters, the data are fit to a scattering function. A semiempirical scattering function, Broad Peak or Polyelectrolyte model, a convolution of form and structure factors, is frequently used to describe systems that exhibit electrostatically driven assembly, such as semidilute polyelectrolyte solutions with low levels of added salt.[44,45] While PCPDTBT-SO_3K is expect to assemble in a similar fashion to other systems governed by electrostatically driven microphase separation, ionic clusters of pendant ionic groups and counterions are anticipated to have an important contribution to the structure factor. Thus, an ionic correlation correction was added to the model to capture that behavior, in the form of an additional Lorentzian-like function, without which the Polyelectrolyte model does not adequately fit the data (Figure 5). The resulting scattering function, a Conjugated Polyelectrolyte model, is given by

$$I(q) = \frac{A}{q^n} + \frac{B}{1 + (|q - q^*|L_{chain})^m} + \frac{C}{1 + (|q - q_{ion}|L_{ion})^p} + I_{inc} \quad (4)$$

where n is the low-q scaling exponent, m is the polyelectrolyte scaling exponent, p is the ionic aggregate scaling exponent, L_{chain} is the electrostatic screening length of the interchain correlation, L_{ion} is the electrostatic screening length of the ionic aggregate correlations, q^* is the interchain correlation peak position, q_{ion} is the ionic aggregate correlation peak position, and I_{inc} is the background incoherent scattering. Real space correlation distances are extracted from these peak positions by $\xi = 2\pi/q$. A, B, and C are scaling factors, dependent on the concentration and scattering length density difference associated with each feature. The exponents n, m, and p capture the breadth of the power law and Lorentzian-like functions, where m is inversely related to the Flory exponent (ν) for polymer systems, i.e. $m \sim 1/\nu_{chain}$, where $\nu = 0.5$ corresponds to the θ condition. The Flory exponent corresponds to collective behavior, highlighting the conformation due to the relative importance of polymer−polymer or polymer−solvent interactions. Thus, m need not be constrained to the $m = 1.3$ result from PCPDTBT-SO_3K in dilute solution (0.3% w/v, D_2O), which only corresponded to correlations along a single chain and highlighted the persistence of the polymer. Similarly, the inverse of n can be used as a Flory-like exponent ($\nu_{microgel}$) to envision the conformation of the microgels.

Parameters extracted by fitting the Conjugated Polyelectrolyte model, eq 4, to the scattering functions of PCPDTBT-SO_3K (4.0% w/v, D_2O) at both temperatures are included in the Supplementary Information. Calculated structural parameters are summarized in Table 1.

Table 1. Structural Parameters of PCPDTBT-SO_3K (4.0% w/v, D_2O) at 25 and 75 °C

parameter	25 °C	75 °C
$\nu_{microgel}$	0.39 ± 0.003	0.39 ± 0.003
ν_{chain}	0.48 ± 0.04	0.45 ± 0.05
ξ_{chain} (nm)	13.7 ± 0.2	12.8 ± 0.3
L_{chain} (nm)	4.9 ± 0.4	4.3 ± 0.3
ξ_{ion} (nm)	6.6 ± 1.3	6.4 ± 1.2
L_{ion} (nm)	2.0 ± 0.8	1.7 ± 1.2

While the uptick at low-q, corresponding to the onset of power law behavior, is often interpreted as a form of aggregation, it is a standard feature of ionic polymer solutions at low salt concentrations that reveals the long length scale correlations[46] of the three-dimensional microstructure. This has been demonstrated with the Polyelectrolyte model for semidilute low-salt polyelectrolyte solutions exhibiting ordered regions of high polymer density coexisting with disordered regions of low polymer content[44,47] and is believed to be related to the attractive electrostatic correlations, independent of backbone hydrophobicity or solvation.[48]

The clusters are compact, collapsed structures, characterized by a Flory-like exponent of 0.39 ± 0.003 that percolate through the disordered low polymer concentration solution forming a network. The microgels are composed of an entangled polyelectrolyte mesh with correlations revealed by the peak present in the mid-q region of the scattering pattern. In the semidilute regime, these polymer chains are interacting, thus yielding interchain correlations but are not dominated by entanglements as in the melt or concentrated solution. This interchain correlation peak at q* is believed to be the well-known polyelectrolyte peak, although there is no direct evidence presented here. The polyelectrolyte peak is caused by local chain rigidification derived from like-charge repulsion of highly charged polymer chains and is seen in various polyelectrolyte systems through light, X-ray, and neutron scattering.[49−57] For PCPDTBT-SO_3K at 25 °C, there exists a statistical correlation length, ξ_{chain}, of (13.7 ± 0.2) nm separating the polymer chains and an electrostatic screening length, L_{chain}, of (4.9 ± 0.4) nm around which each chain can be felt.

The correlation length, ξ_{chain}, can be compared to the scaling relationship[58,59] for the correlation length of a polyelectrolyte incorporating electrostatic and entropic chain conformation effects:

$$\xi \approx f^{-2/7}\left(\frac{l_B}{b}\right)^{-1/7}(bC)^{-1/2} \quad (5)$$

DOI: 10.1021/acs.chemmater.7b05303
Chem. Mater. 2018, 30, 1417−1426

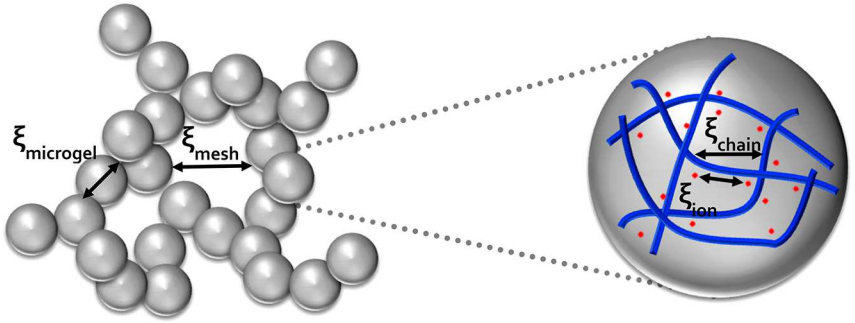

Figure 6. Proposed hierarchical structure of PCPDTBT-SO_3K hydrogels, highlighting the void size (ξ_{mesh}), dimension of the microgel particle ($\xi_{microgel}$), and correlation lengths between chains (ξ_{chain}) and ionic clusters (ξ_{ion}).

where f is the fraction of charged monomers, l_B is the Bjerrum length, the length at which electrostatic interaction energy is equal to the thermal energy k_BT, b is the monomer size, and C is the polymer concentration. Taking into account counterion condensation,[60] the polyelectrolyte chain and condensed counterions are equivalent to a polyelectrolyte with charges l_B apart. Because the fraction of charged monomers is experimentally controlled as $f = b/l_B$, the resulting correlation length[61] is given by

$$\xi \approx \left(\frac{l_B}{b}\right)^{1/7} (bC)^{-1/2} \tag{6}$$

which agrees well with the experimentally determined mesh size and corroborates the presented description of the CPE hydrogel as a polyelectrolyte in semidilute solution. The larger value of L_{chain} compared to other polyelectrolytes such as PSS[57] is likely due to both the finite thickness of the PCPDTBT-SO_3K chain and the increased backbone stiffness from the fused ring conjugated backbone.

These scaling relationships (eqs 5 and 6) not only give qualitative agreement with the hierarchical structure of the PCPDTBT-SO_3K hydrogels presented here but also provide insights into the molecular design of CPEs. Compared to traditional polyelectrolytes, CPEs allow these parameters (f, b, and l_B) to span a greater breadth of values. Owing to the combination of highly polarizable backbone, pendant ionic groups, and nonpolar alkyl side chain linkers, CPEs are soluble in a range of solvent conditions, typically with larger Bjerrum lengths, allowing larger correlation lengths. Additionally, the monomer size in CPEs is typically also much larger (~1.2 nm for PCPDTBT backbones) and can be tuned easily through the addition of different donor or acceptor moieties. Control of these two parameters should allow design of CPEs with precisely tunable polyelectrolyte mesh spacing. Further, due to the interplay of these two parameters, CPEs significantly delay the onset of counterion condensation as the Bjerrum length is increased, enabling dissociated ions and electrostatic behavior in low dielectric solvents.

Ion−ion correlations or ionic aggregates present in the entangled polyelectrolyte mesh appear at progressively shorter length scales. This weak, secondary correlation appears as a shoulder of the more pronounced polyelectrolyte correlation in the scattering function of Figure 5. The ionic aggregates (with scattering contrast including both the pendant ionic sulfonate groups and potassium counterions) are correlated with a characteristic spacing, ξ_{ion}, (6.6 ± 1.3) nm of between aggregates, which is on order of the chain length rather than the monomer scale. As such, it is believed these ionic aggregates help to tie separate chains together as dynamic physical cross-links. The screening length, L_{ion}, of (2.0 ± 0.8) nm is interpreted as a characteristic length scale for electrostatic screening between ions and is related to the dielectric constant of the medium, the concentration of ionic species, and the number of ions associating in each ionic aggregate.

As the temperature is increased from 25 to 75 °C, the overall hierarchical structure (Figure 6) remains intact, but there is a compaction of both the entangled polyelectrolyte mesh and ionic correlations (Table 1). The percolated three-dimensional network of clustered microgels shows only minor changes, a surprising result as the macroscopic mechanical properties shift from elastic to viscous response. The Flory-like exponents characterizing the cluster morphology and interchain correlations remain effectively constant, demonstrating no detectable change in conformation. The correlation and screening lengths show compaction for the interchain correlations: ξ_{chain} falls from (13.7 ± 0.2) to (12.8 ± 0.3) nm and L_{chain} decreases from (4.9 ± 0.4) to (4.3 ± 0.3) nm. While the ion correlations follow similar behavior, it is hard to make quantitative statements as relatively weak scattering results in high uncertainty of the fits.

X-ray scattering studies aid in investigating the ionic interactions, as improved signal intensity results from an increased electron density contrast between the ionic moieties relative to the polymer and solvent, and better temperature resolution is experimentally accessible in understanding the structural transitions. Figure 7 summarizes the small-angle X-ray scattering (SAXS) profiles for PCPDTBT-SO_3K (4.0% w/v, H_2O) from 25 to 75 °C.

Strikingly, the disordering of the microgel morphology begins at the reorganization temperature determined by WAXS, at which the dissociation of ionic cross-links and increase in polymer solvation occurs: 45−50 °C. Nonetheless, the microgels continue to lose structure with further heating. The polyelectrolyte peak, as probed by SAXS, is more diffuse and at lower-q than from SANS, which we attribute to differences in scattering length density probing slightly different correlations. While it appears that the polyelectrolyte peak shifts to higher q, indicating the collapse of the entangled polyelectrolyte mesh network, the predominant effect is the collapse in intensity of the peak, due to a loss of correlations. This apparently reflects increased solvation of the CPE chains and associated counterions, which are then able to access more conformations, resulting in a smearing of the network structure. Further, the thermoresponsive character is reversible, highlighting an equilibrated system; the structure and properties (i.e., rheology, conductivity) can be recovered given sufficient equilibration at any temperature.

DOI: 10.1021/acs.chemmater.7b05303
Chem. Mater. 2018, 30, 1417−1426

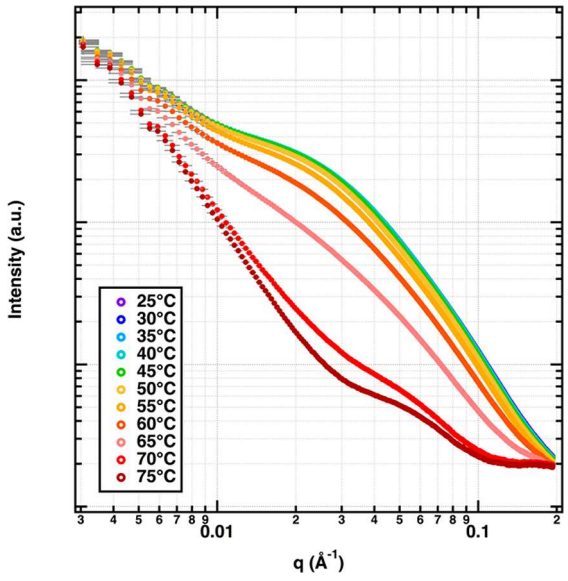

Figure 7. SAXS data for PCPDTBT-SO_3K hydrogels (4.0% w/v, H_2O) from 25 to 75 °C. Outside of low-q data points, error bars are smaller than markers. Data from 25 to 40 °C are coincident and are hidden behind the 45 °C data.

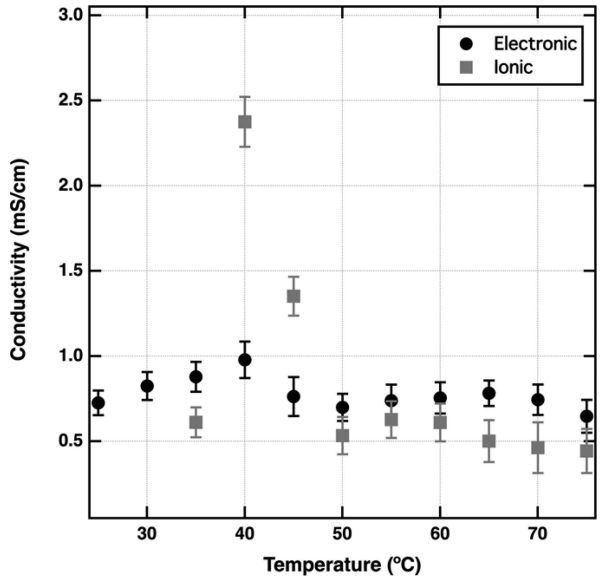

Figure 8. Electronic (●) and ionic (■) conductivities of PCPDTBT-SO3K hydrogels (4.0% w/v, H_2O) as a function of increasing temperature.

Structural Effects on Conductivity. Importantly, the PCPDTBT-SO_3K hydrogels remain semiconducting, as revealed in Figure 8 (determined by electrochemical impedance spectroscopy with an in-plane geometry). The system exhibits particularly high conductivities (~0.5−2.5 mS/cm) given the lack of evidence for crystallinity, $\pi-\pi$ stacking, or other well-defined aromatic interactions and the extremely high (96%) water content. At the lowest temperatures (25 to 30 °C), the charge transport is dominated by electronic conductivity, with the ions effectively frozen within the ionic aggregates. As the temperature is increased (40−45 °C), the ionic conductivity sharply increases as the ions gain mobility due to dissociation of ionic cross-links and release of unbound counterions. At elevated temperatures (>50 °C), the ionic conductivity drops back and plateaus at a comparable level to the electronic conductivity: a saturation attributed to a concomitant loss in percolation pathways for the ions. It is expected that both electronic and ionic conduction primarily occur through pathways in the microgels due to the higher local concentration of mobile charge carriers within the clusters. Moreover, for electronic conduction, there must still be an appreciable amount of π-orbital overlap where there are interchain connections so that holes can hop between adjacent chains.

In designing new mixed conductor hydrogels based on CPEs, there are several important principles that can be elucidated or anticipated from this investigation. Increasing the polymer concentration should lead to higher conductivities due to increased contact of the electrodes with the electroactive microgel cluster and increased percolation of the microgel clusters. Manipulating the solvent dielectric properties could allow for conduction outside the clusters and affect the formation of ionic aggregates. Strategies to incorporate $\pi-\pi$ stacking through processing, materials design, or solvent control could have important effects on transport.

■ CONCLUSIONS

PCPDTBT-SO_3K, a high-mobility CPE, undergoes solution assembly and solidification driven primarily by electrostatics, rather than $\pi-\pi$ stacking, forming a three-dimensional network with a novel, hierarchical structure (Figure 6). A percolated network exists at large distances, composed of microgel clusters that are aggregated at ambient temperatures but become electrostatically stabilized at higher temperatures as ions gain mobility out of the ionic aggregates toward the surface of the microgel. The interiors of these microgel clusters are entangled polyelectrolyte meshes that behave predominantly like classical polyelectrolytes in the semidilute regime without added salt but additionally incorporate unstructured aromatic interactions and ionic aggregate cross-links. The organization of CPEs in this regime is free from $\pi-\pi$ stacking, with implications for CPE hydrogels and solution assemblies relying predominantly on intrachain charge transfer. Future work should be aimed at elucidating mechanisms for control of ionic aggregates, percolation of the microgel network, and $\pi-\pi$ stacking, especially in added salt regimes.

■ EXPERIMENTAL SECTION

Materials. Milli-Q ultrapure water (18.2 M Ω·cm at 25 °C) was used for the preparation of all aqueous samples and in all synthetic procedures. All chemicals, unless otherwise noted, were commercially available and used as received from Sigma-Aldrich. Deuterated solvents were obtained from Cambridge Isotope Laboratories.

PCPDTBT-SO_3K was synthesized according to literature procedures.[20] The molecular weight and dispersity of PCPDTBT-SO_3K were determined by gel permeation chromatography in DMF of its derivative, resulting from exhaustive ion exchange with excess tetrabutylammonium bromide, followed by dialysis.[20]

Molecular Characterization. ^{1}H NMR spectra were recorded at either 500 MHz (Bruker AVANCE500) or 600 MHz (Varian VNMRS), and ^{13}C NMR spectra were recorded at either 126 MHz (Bruker AVANCE500) or 150 MHz (Varian VNMRS) in D_2O or DMSO-d_6. Chemical shifts are reported in ppm referenced to residual solvent peaks. Gel permeation chromatography (GPC) was conducted on a Waters instrument using a refractive index detector and Viscotek Visco Gel I-Series columns (IMBHMW-3078, IMBLMW-3078). DMF with 0.1% LiBr at 25 °C was used as the mobile phase with a flow rate of 1 mL/min. Reported molecular weight and dispersity (Đ) values are relative to polystyrene (PS) equivalents as calibrated with narrow PS Standards (Agilent). Mass analysis was performed using electrospray

DOI: 10.1021/acs.chemmater.7b05303
Chem. Mater. 2018, 30, 1417−1426

ionization methods (ESI) using a Waters Micromass QTOF2 mass spectrometer. Elemental analysis using the Dumas method was performed on a Control Equipment Corp. instrument (CEC 440HA).

Electron Microscopy. FF-SEM experiments were conducted on a FEI XL30 microscope operating at an acceleration voltage of 10.0 kV. Freeze-fractured samples were prepared with a Quorum Technologies Polaron PP2000T cryo-stage. The stage was cooled to the temperature of liquid nitrogen. Then, a small volume of solution was added and rapidly cooled by liquid nitrogen, allowing vitrified amorphous water, avoiding ice crystallization and preserving the native structure of the solution.[62] The samples were put under vacuum at continuous cooling with liquid nitrogen and fractured with a microtome knife. The surface was replicated by coating with Pt at an angle of 90°.

Rheology. Rheological measurements were taken on an AR-G2 rheometer using 20 mm diameter stainless steel parallel plates with a 200 μm gap. Sample environment was controlled by using a Peltier-controlled lower plate for temperature control and covering the fixture to prevent ambient humidity from affecting the measurements. Dynamic strain sweeps were performed at 1 and 10 rad s^{-1} to determine the linear viscoelastic regime, where the upper limit of the linear viscoelastic regime is defined as the critical strain (γ_c), below which the dynamic modulus remains invariant. The γ_c for the PCPDTBT-SO_3K hydrogel (4.0% w/v, H_2O) at 25 °C was approximately 5% (Figure S2). All further measurements were taken at 1% strain to remain within the linear viscoelastic regime.

X-ray Scattering. PCPDTBT-SO_3K was dissolved in Milli-Q ultrapure water at the appropriate concentrations (0.3 and 4.0% w/v). Vortexing, sonication, and mild heating were used to aid in dissolution. Solutions were loaded into Kapton lined 1 mm-thick aluminum washers, sealed, and allowed to equilibrate for 72 h at ambient conditions before measurement. Sample cells were loaded in a temperature-controlled sample holder and allowed to equilibrate for 15 min at each temperature before exposure. Before measurement, the sample was heated above room temperature and then equilibrated at 25 °C for 30 min to remove any thermal history effects. The presented data are from a single cycle of monotonic heating from 25 to 75 °C but are reproducible upon significant equilibration (up to 24 h from 75 °C back to 25 °C).

SAXS patterns were obtained at beamline 7.3.3 of the Advanced Light Source (ALS) at Lawrence Berkeley National Laboratory in Berkeley, CA.[63] A sample−detector distance of 3770 mm was used with an X-ray beam energy of 10.0 keV corresponding to a wavelength, λ, of 1.24 Å. Scattering angles were calibrated to a silver behenate (AgB) standard. WAXS patterns were obtained at beamline 11-3 of the Stanford Synchrotron Radiation Lightsource (SSRL) in Menlo Park, CA. A sample−detector distance of 369 mm was used with an X-ray wavelength, λ, of 1 Å corresponding to a beam energy of 12.4 keV. Scattering angles were calibrated to a lanthanum hexaboride (LaB_6) standard. Data were reduced using the Nika package for Igor.[64] The scattered intensity, $I(q)$, was obtained by circular averaging of the intensity.

Neutron Scattering. SANS studies were conducted on the NGB-30 instrument at the National Institute of Standards and Technology Center for Neutron Research (NCNR) in Gaithersburg, MD.[65] Three sample−detector distances were used (1.3, 4, and 13 m) with a neutron beam wavelength, λ, of 6 Å, yielding a q range of (0.003433−0.4121) $Å^{-1}$, where the scattering variable is $q = (4\pi/\lambda)\sin(\theta/2)$ and θ is the scattering angle. The scattered intensity, $I(q)$, was obtained by circular averaging of the intensity. Typical empty cell and blocked beam corrections were made. Averaged data were placed on an absolute cross-sectional scale.

PCPDTBT-SO_3K was dissolved in D_2O at the appropriate concentrations (0.3 and 4.0% w/v). Vortexing, sonication, and mild heating were used to aid in dissolution. Solutions were placed into titanium sample cells with quartz windows and a 1 mm path length and allowed to equilibrate for 72 h at ambient conditions before measurement. Sample cells were loaded in a temperature-controlled sample holder of ±0.1 °C and allowed to equilibrate for 1 h at each temperature. Data reduction followed typical procedures using the NCNR SANS packages for Igor.[66]

Electrochemical Impedance Spectroscopy. Impedance measurements were taken on a Biologic VSP-300 potentiostat using an in-plane configuration. Sample was deposited onto a glass substrate with evaporated gold contacts. The electroactive area of the sample was controlled through a layer of Kapton tape, with a well of defined area. The lateral dimensions were measured with a digital micrometer, and the thickness of the gel sample was calculated from the volume deposited. The impedance measurements were performed from 7 MHz to 1 Hz with a sinusoidal amplitude of 100 mV, using an INSTEC stage (±0.1 °C accuracy) to control the temperature of the sample. The conductivity was monitored until stabilized at each temperature. The presented data are from a single cycle of monotonic heating from 25 to 75 °C but are reproducible upon significant equilibration (up to 24 h from 75 °C back to 25 °C).

Given the interactions between electronic and ionic charge carriers, especially in an inhomogeneous dielectric continuum (i.e., the hierarchical three-dimensional network structure, composing PCPDTBT-SO_3K chains, counterions, and solvent both inside the microgels and in the void spaces), it is not currently possible to fit the data to an appropriate equivalent circuit model. To obtain estimates of the ionic and electronic conductivities, the frequency independent plateaus (Figure S6) of impedance were converted to conductivity according to

$$\sigma = \frac{l}{|Z^*|tw} \tag{7}$$

where $|Z^*|$ is the total impedance, t is the thickness of the sample, w is the lateral sample width, and l is the distance between electrodes and taken as the DC conductivities. The total impedance of the high frequency plateau is taken as the electronic resistance and is used to calculate the electronic conductivity. The impedance of the low frequency plateau is taken as the sum of ionic and electronic resistances. Subtracting the electronic contribution to this impedance, the ionic conductivity can be calculated according to eq 7. Noteworthy, this approach likely significantly underestimates the conductivities by neglecting contact resistance between the sample and the electrodes, which would be present in both plateaus in the Bode plots (Figure S6).

■ ASSOCIATED CONTENT

Supporting Information

The Supporting Information is available free of charge on the ACS Publications website at DOI: 10.1021/acs.chemmater.7b05303.

Experimental details, characterization data, and SANS fit parameters and theoretical background (PDF)

■ AUTHOR INFORMATION

Corresponding Authors

*E-mail: ghf@ucsb.edu (G.H.F.).
*E-mail: segalman@ucsb.edu (R.A.S.).

ORCID

Scott P. O. Danielsen: 0000-0003-3432-5578
Guillermo C. Bazan: 0000-0002-2537-0310
Glenn H. Fredrickson: 0000-0002-6716-9017
Rachel A. Segalman: 0000-0002-4292-5103

Present Address

¶G.E.S.: Sciences et Ingénierie de la Matière Molle, CNRS UMR 7615, École Supérieure de Physique et de Chemie Industrielles de la Ville de Paris (ESPCI), ParisTech, PSL Research University, 10 Rue Vauquelin, Paris, Cedex 05 F-7523, France.

Notes

The authors declare no competing financial interest.

DOI: 10.1021/acs.chemmater.7b05303
Chem. Mater. 2018, 30, 1417−1426

■ ACKNOWLEDGMENTS

We gratefully acknowledge support from the NSF Polymers Program under Award DMR 1608297 for all work on synthesis, characterization, and analysis. G.E.S. gratefully acknowledges the AFOSR MURI program under FA9550-12-1 for financial support of X-ray scattering measurements. Access to the NGB-30m SANS instrument was provided by the Center for High Resolution Neutron Scattering, a partnership between the National Institute of Standards and Technology and the National Science Foundation Agreement DMR-1508249. We acknowledge the support of the National Institute of Standards and Technology, U.S. Department of Commerce, in providing the neutron research facilities used in this work. Use of the Stanford Synchrotron Radiation Lightsource, SLAC National Accelerator Laboratory, is supported by the U.S. Department of Energy, Office of Science, Office of Basic Energy Sciences under Contract DE-AC02-76SF00515. The Advanced Light Source is supported by the Director, Office of Science, Office of Basic Energy Sciences, of the U.S. Department of Energy under Contract DE-AC02-05CH11231.The MRL Shared Experimental Facilities are supported by the MRSEC Program of the NSF under Award DMR 1720256; a member of the NSF-funded Materials Research Facilities Network. The authors additionally thank Yun Liu at the NIST Center for Neutron Research for helpful discussions in planning the neutron experiments, Kris Delaney at UCSB for helpful discussions in understanding the scattering functions, and Sage Davis at UCSB for assistance in obtaining microscopy images. The identification of commercial products does not imply endorsement by the National Institute of Standards and Technology nor does it imply that these are the best for the purpose.

■ REFERENCES

(1) Pinto, M. R.; Schanze, K. S. Conjugated polyelectrolytes: Synthesis and applications. *Synthesis* **2002**, *2002*, 1293−1309.
(2) Kirchhofer, N. D.; McCuskey, S. R.; Mai, C. K.; Bazan, G. C. Anaerobic Respiration on Self-Doped Conjugated Polyelectrolytes: Impact of Chemical Structure. *Angew. Chem., Int. Ed.* **2017**, *56*, 6519−6522.
(3) Rivnay, J.; Owens, R. M.; Malliaras, G. G. The Rise of Organic Bioelectronics. *Chem. Mater.* **2014**, *26*, 679−685.
(4) Yan, H. J.; Chuang, C.; Zhugayevych, A.; Tretiak, S.; Dahlquist, F. W.; Bazan, G. C. Inter-Aromatic Distances in Geobacter Sulfurreducens Pili Relevant to Biofilm Charge Transport. *Adv. Mater.* **2015**, *27*, 1908−1911.
(5) Hoven, C. V.; Garcia, A.; Bazan, G. C.; Nguyen, T. Q. Recent Applications of Conjugated Polyelectrolytes in Optoelectronic Devices. *Adv. Mater.* **2008**, *20*, 3793−3810.
(6) Liu, B.; Wang, S.; Bazan, G. C.; Mikhailovsky, A. Shape-adaptable water-soluble conjugated polymers. *J. Am. Chem. Soc.* **2003**, *125*, 13306−13307.
(7) Brookins, R. N.; Schanze, K. S.; Reynolds, J. R. Base-free Suzuki polymerization for the synthesis of polyfluorenes functionalized with carboxylic acids. *Macromolecules* **2007**, *40*, 3524−3526.
(8) Gaylord, B. S.; Heeger, A. J.; Bazan, G. C. DNA detection using water-soluble conjugated polymers and peptide nucleic acid probes. *Proc. Natl. Acad. Sci. U. S. A.* **2002**, *99*, 10954−10957.
(9) Gaylord, B. S.; Heeger, A. J.; Bazan, G. C. DNA hybridization detection with water-soluble conjugated polymers and chromophore-labeled single-stranded DNA. *J. Am. Chem. Soc.* **2003**, *125*, 896−900.
(10) Wang, D. L.; Gong, X.; Heeger, P. S.; Rininsland, F.; Bazan, G. C.; Heeger, A. J. Biosensors from conjugated polyelectrolyte complexes. *Proc. Natl. Acad. Sci. U. S. A.* **2002**, *99*, 49−53.
(11) Liu, B.; Bazan, G. C. Homogeneous fluorescence-based DNA detection with water-soluble conjugated polymers. *Chem. Mater.* **2004**, *16*, 4467−4476.
(12) Liu, B.; Bazan, G. C. Interpolyelectrolyte complexes of conjugated copolymers and DNA: Platforms for multicolor biosensors. *J. Am. Chem. Soc.* **2004**, *126*, 1942−1943.
(13) Tian, J.; Wu, C. C.; Thompson, M. E.; Sturm, J. C.; Register, R. A. Photophysical Properties, Self-Assembled Thin-Films, and Light-Emitting-Diodes of Poly(P-Pyridylvinylene)S and Poly(P-Pyridinium Vinylene)S. *Chem. Mater.* **1995**, *7*, 2190−2198.
(14) Thunemann, A. F. Nanostructured dihexadecyldimethylammonium-poly(1,4-phenylene-ethinylene-carboxylate): An ionic complex with blue electroluminescence. *Adv. Mater.* **1999**, *11*, 127−130.
(15) Cimrova, V.; Remmers, M.; Neher, D.; Wegner, G. Polarized light emission from LEDs prepared by the Langmuir-Blodgett technique. *Adv. Mater.* **1996**, *8*, 146−149.
(16) Tada, K.; Onoda, M.; Hirohata, M.; Kawai, T.; Yoshino, K. Blue-green electroluminescence in copolymer based on poly(1,4-phenylene ethynylene). *Jpn. J. Appl. Phys., Part 2* **1996**, *35*, L251−L253.
(17) Seo, J. H.; Namdas, E. B.; Gutacker, A.; Heeger, A. J.; Bazan, G. C. Solution-Processed Organic Light-Emitting Transistors Incorporating Conjugated Polyelectrolytes. *Adv. Funct. Mater.* **2011**, *21*, 3667−3672.
(18) Mai, C. K.; Schlitz, R. A.; Su, G. M.; Spitzer, D.; Wang, X. J.; Fronk, S. L.; Cahill, D. G.; Chabinyc, M. L.; Bazan, G. C. Side-Chain Effects on the Conductivity, Morphology, and Thermoelectric Properties of Self-Doped Narrow-Band-Gap Conjugated Polyelectrolytes. *J. Am. Chem. Soc.* **2014**, *136*, 13478−13481.
(19) Mai, C. K.; Arai, T.; Liu, X. F.; Fronk, S. L.; Su, G. M.; Segalman, R. A.; Chabinyc, M. L.; Bazan, G. C. Electrical properties of doped conjugated polyelectrolytes with modulated density of the ionic functionalities. *Chem. Commun.* **2015**, *51*, 17607−17610.
(20) Mai, C. K.; Zhou, H. Q.; Zhang, Y.; Henson, Z. B.; Nguyen, T. Q.; Heeger, A. J.; Bazan, G. C. Facile Doping of Anionic Narrow-Band-Gap Conjugated Polyelectrolytes During Dialysis. *Angew. Chem., Int. Ed.* **2013**, *52*, 12874−12878.
(21) Choi, H.; Mai, C. K.; Kim, H. B.; Jeong, J.; Song, S.; Bazan, G. C.; Kim, J. Y.; Heeger, A. J. Conjugated polyelectrolyte hole transport layer for inverted-type perovskite solar cells. *Nat. Commun.* **2015**, *6*, 7348−7353.
(22) Zhou, H. Q.; Zhang, Y.; Mai, C. K.; Collins, S. D.; Nguyen, T. Q.; Bazan, G. C.; Heeger, A. J. Conductive Conjugated Polyelectrolyte as Hole-Transporting Layer for Organic Bulk Heterojunction Solar Cells. *Adv. Mater.* **2014**, *26*, 780−785.
(23) Zhou, H. Q.; Zhang, Y.; Mai, C. K.; Collins, S. D.; Bazan, G. C.; Nguyen, T. Q.; Heeger, A. J. Polymer Homo-Tandem Solar Cells with Best Efficiency of 11.3%. *Adv. Mater.* **2015**, *27*, 1767−1773.
(24) Zhou, H. Q.; Zhang, Y.; Mai, C. K.; Seifter, J.; Nguyen, T. Q.; Bazan, G. C.; Heeger, A. J. Solution-Processed pH-Neutral Conjugated Polyelectrolyte Improves Interfacial Contact in Organic Solar Cells. *ACS Nano* **2015**, *9*, 371−377.
(25) Knaapila, M.; Monkman, A. P. Methods for Controlling Structure and Photophysical Properties in Polyfluorene Solutions and Gels. *Adv. Mater.* **2013**, *25*, 1090−1108.
(26) Newbloom, G. M.; Weigandt, K. M.; Pozzo, D. C. Electrical, Mechanical, and Structural Characterization of Self-Assembly in Poly(3-hexylthiophene) Organogel Networks. *Macromolecules* **2012**, *45*, 3452−3462.
(27) Newbloom, G. M.; Weigandt, K. M.; Pozzo, D. C. Structure and property development of poly(3-hexylthiophene) organogels probed with combined rheology, conductivity and small angle neutron scattering. *Soft Matter* **2012**, *8*, 8854−8864.
(28) Wang, D. L.; Lal, J.; Moses, D.; Bazan, G. C.; Heeger, A. J. Small angle neutron scattering (SANS) studies of a conjugated polyelectrolyte in aqueous solution. *Chem. Phys. Lett.* **2001**, *348*, 411−415.
(29) Wang, D. L.; Moses, D.; Bazan, G. C.; Heeger, A. J.; Lal, J. Conformation of a conjugated polyelectrolyte in aqueous solution: Small angle neutron scattering. *J. Macromol. Sci., Part A: Pure Appl.Chem.* **2001**, *38*, 1175−1189.

DOI: 10.1021/acs.chemmater.7b05303
Chem. Mater. 2018, 30, 1417−1426

(30) Huber, R. C.; Ferreira, A. S.; Aguirre, J. C.; Kilbride, D.; Toso, D. B.; Mayoral, K.; Zhou, Z. H.; Kopidakis, N.; Rubin, Y.; Schwartz, B. J.; Mason, T. G.; Tolbert, S. H. Structure and Conductivity of Semiconducting Polymer Hydrogels. *J. Phys. Chem. B* **2016**, *120*, 6215−6224.
(31) Pellet, C.; Cloitre, M. The glass and jamming transitions of soft polyelectrolyte microgel suspensions. *Soft Matter* **2016**, *12*, 3710−3720.
(32) Kratky, O.; Porod, G. Diffuse Small-Angle Scattering of X-Rays in Colloid Systems. *J. Colloid Sci.* **1949**, *4*, 35−70.
(33) Saito, N.; Takahashi, K.; Yunoki, Y. Statistical Mechanical Theory of Stiff Chains. *J. Phys. Soc. Jpn.* **1967**, *22*, 219−226.
(34) Pedersen, J. S.; Schurtenberger, P. Scattering functions of semiflexible polymers with and without excluded volume effects. *Macromolecules* **1996**, *29*, 7602−7612.
(35) Chen, W. R.; Butler, P. D.; Magid, L. J. Incorporating intermicellar interactions in the fitting of SANS data from cationic wormlike micelles. *Langmuir* **2006**, *22*, 6539−6548.
(36) Fetters, L. J.; Lohse, D. J.; Richter, D.; Witten, T. A.; Zirkel, A. Connection between Polymer Molecular-Weight, Density, Chain Dimensions, and Melt Viscoelastic Properties. *Macromolecules* **1994**, *27*, 4639−4647.
(37) McCulloch, B.; Ho, V.; Hoarfrost, M.; Stanley, C.; Do, C.; Heller, W. T.; Segalman, R. A. Polymer Chain Shape of Poly(3-alkylthiophenes) in Solution Using Small-Angle Neutron Scattering. *Macromolecules* **2013**, *46*, 1899−1907.
(38) Gettinger, C. L.; Heeger, A. J.; Drake, J. M.; Pine, D. J. A Photoluminescence Study of Poly(Phenylene Vinylene) Derivatives - the Effect of Intrinsic Persistence Length. *J. Chem. Phys.* **1994**, *101*, 1673−1678.
(39) Gettinger, C. L.; Heeger, A. J.; Drake, J. M.; Pine, D. J. The Effect of Intrinsic Rigidity on the Optical-Properties of PPV Derivatives. *Mol. Cryst. Liq. Cryst. Sci. Technol., Sect. A* **1994**, *256*, 507−512.
(40) Fytas, G.; Nothofer, H. G.; Scherf, U.; Vlassopoulos, D.; Meier, G. Structure and dynamics of nondilute polyfluorene solutions. *Macromolecules* **2002**, *35*, 481−488.
(41) Murnen, H. K.; Rosales, A. M.; Dobrynin, A. V.; Zuckermann, R. N.; Segalman, R. A. Persistence length of polyelectrolytes with precisely located charges. *Soft Matter* **2013**, *9*, 90−98.
(42) Ying, Q. C.; Chu, B. Overlap Concentration of Macromolecules in Solution. *Macromolecules* **1987**, *20*, 362−366.
(43) Doi, M.; Edwards, S. F. Dynamics of Rod-Like Macromolecules in Concentrated-Solution 0.2. *J. Chem. Soc., Faraday Trans. 2* **1978**, *74*, 918−932.
(44) Horkay, F.; Hammouda, B. Small-angle neutron scattering from typical synthetic and biopolymer solutions. *Colloid Polym. Sci.* **2008**, *286*, 611−620.
(45) Murphy, R. J.; Weigandt, K. M.; Uhrig, D.; Alsayed, A.; Badre, C.; Hough, L.; Muthukumar, M. Scattering Studies on Poly(3,4-ethylenedioxythiophene)-Polystyrenesulfonate in the Presence of Ionic Liquids. *Macromolecules* **2015**, *48*, 8989−8997.
(46) Wiltzius, P.; Haller, H. R.; Cannell, D. S.; Schaefer, D. W. Dynamics of Long-Wavelength Concentration Fluctuations in Solutions of Linear-Polymers. *Phys. Rev. Lett.* **1984**, *53*, 834−837.
(47) Matsuoka, H.; Schwahn, D.; Ise, N. Observation of Cluster Formation in Polyelectrolyte Solutions by Small-Angle Neutron-Scattering 0.1. A Steep Upturn of the Scattering Curves from Solutions of Sodium Poly(Styrenesulfonate) at Scattering Vectors Below 0.01(a)-1. *Macromolecules* **1991**, *24*, 4227−4228.
(48) Ermi, B. D.; Amis, E. J. Influence of backbone solvation on small angle neutron scattering from polyelectrolyte solutions. *Macromolecules* **1997**, *30*, 6937−6942.
(49) Degennes, P. G.; Pincus, P.; Velasco, R. M.; Brochard, F. Remarks on Polyelectrolyte Conformation. *J. Phys. (Paris)* **1976**, *37*, 1461−1473.
(50) Nierlich, M.; Williams, C. E.; Boue, F.; Cotton, J. P.; Daoud, M.; Famoux, B.; Jannink, G.; Picot, C.; Moan, M.; Wolff, C.; Rinaudo, M.; de Gennes, P. G. Small-Angle Neutron-Scattering by Semi-Dilute Solutions of Polyelectrolyte. *J. Phys. (Paris)* **1979**, *40*, 701−704.
(51) Ise, N.; Okubo, T. Ordered Distribution of Electrically Charged Solutes in Dilute-Solutions. *Acc. Chem. Res.* **1980**, *13*, 303−309.
(52) Ise, N.; Okubo, T.; Kunugi, S.; Matsuoka, H.; Yamamoto, K.; Ishii, Y. Ordered Structure in Dilute-Solutions of Sodium Polystyrenesulfonates as Studied by Small-Angle X-Ray-Scattering. *J. Chem. Phys.* **1984**, *81*, 3294−3306.
(53) Ise, N.; Okubo, T.; Yamamoto, K.; Matsuoka, H.; Kawai, H.; Hashimoto, T.; Fujimura, M. Ordered Structure in Dilute-Solutions of Poly-L-Lysine as Studied by Small-Angle X-Ray-Scattering. *J. Chem. Phys.* **1983**, *78*, 541−545.
(54) Drifford, M.; Dalbiez, J. P. Light-Scattering by Dilute-Solutions of Salt-Free Poly-Electrolytes. *J. Phys. Chem.* **1984**, *88*, 5368−5375.
(55) Nierlich, M.; Boue, F.; Lapp, A.; Oberthur, R. Characteristic Lengths and the Structure of Salt Free Polyelectrolyte Solutions - a Small-Angle Neutron-Scattering Study. *Colloid Polym. Sci.* **1985**, *263*, 955−964.
(56) Borsali, R.; Nguyen, H.; Pecora, R. Small-angle neutron scattering and dynamic light scattering from a polyelectrolyte solution: DNA. *Macromolecules* **1998**, *31*, 1548−1555.
(57) Prabhu, V. M.; Muthukumar, M.; Wignall, G. D.; Melnichenko, Y. B. Polyelectrolyte chain dimensions and concentration fluctuations near phase boundaries. *J. Chem. Phys.* **2003**, *119*, 4085−4098.
(58) Barrat, J. L.; Joanny, J. F. Theory of polyelectrolyte solutions. *Adv. Chem. Phys.* **2007**, *94*, 1−66.
(59) Dobrynin, A. V.; Colby, R. H.; Rubinstein, M. Scaling Theory of Polyelectrolyte Solutions. *Macromolecules* **1995**, *28*, 1859−1871.
(60) Manning, G. S. Limiting Laws and Counterion Condensation in Polyelectrolyte Solutions.I. Colligative Properties. *J. Chem. Phys.* **1969**, *51*, 924−931.
(61) Vallat, P.; Catala, J. M.; Rawiso, M.; Schosseler, F. Flexible conjugated polyelectrolyte solutions: A small angle scattering study. *Macromolecules* **2007**, *40*, 3779−3783.
(62) Severs, N. J. Freeze-fracture electron microscopy. *Nat. Protoc.* **2007**, *2*, 547−576.
(63) Hexemer, A. B. W.; Glossinger, J.; Schaible, E.; Gann, E.; Kirian, R.; MacDowell, A.; Church, M.; Rude, B.; Padmore, H. In *A SAXS/WAXS/GISAXS Beamline with Multilayer Monochromator*, 14th International Conference on Small-Angle Scattering (SAS09), September 13−18, 2009; IOP Publishing Ltd.: Oxford, England, 2009.
(64) Ilavsky, J. Nika: software for two-dimensional data reduction. *J. Appl. Crystallogr.* **2012**, *45*, 324−328.
(65) Glinka, C. J.; Barker, J. G.; Hammouda, B.; Krueger, S.; Moyer, J. J.; Orts, W. J. The 30 m small-angle neutron scattering instruments at the National Institute of Standards and Technology. *J. Appl. Crystallogr.* **1998**, *31*, 430−445.
(66) Kline, S. R. Reduction and analysis of SANS and USANS data using IGOR Pro. *J. Appl. Crystallogr.* **2006**, *39*, 895−900.

DOI: 10.1021/acs.chemmater.7b05303
Chem. Mater. 2018, 30, 1417−1426